



## A planar thermoelectric power generator for integration in wearable microsystems

João Paulo Carmo<sup>a,\*</sup>, Luis Miguel Goncalves<sup>a</sup>, Reinoud F. Wolffenbuttel<sup>b</sup>, José Higino Correia<sup>a</sup>

<sup>a</sup> University of Minho, Dept Industrial Electronics, Campus Azurem, 4800-058 Guimarães, Portugal

<sup>b</sup> Delft University of Technology, Faculty of EEMCS, Department ME/EL, Mekelweg 4, 2628CD Delft, The Netherlands

### ARTICLE INFO

#### Article history:

Received 9 November 2009

Received in revised form 26 March 2010

Accepted 13 May 2010

Available online 26 May 2010

#### Keywords:

Thermoelectric  
Peltier  
Microcooler  
Telluride  
Energy harvesting

### ABSTRACT

A technique for IC-compatible fabrication of a planar (in-plane) thermoelectric (TE) power generator using a thermopile composed of n-type bismuth telluride ( $\text{Bi}_2\text{Te}_3$ ) and p-type antimony telluride ( $\text{Sb}_2\text{Te}_3$ ) thin-films is presented. The research demonstrates that the thermal co-evaporation of bismuth/antimony (Bi/Sb) and telluride (Te) is the most suitable deposition technique. The measurements showed TE performance properties of the deposited thin-films that are comparable to those reported for the same materials in the bulk form. The measurements showed absolute values of the Seebeck coefficient in the range  $91\text{--}248\text{ }\mu\text{V K}^{-1}$ , an electrical resistivity in the  $7.6\text{--}39.1\text{ }\mu\Omega\text{ m}$  range and a thermal conduction between  $1.3$  and  $1.8\text{ W m}^{-1}\text{ K}^{-1}$ . The best resulting figures-of-merit,  $ZT$ , at room temperatures were  $0.97$  and  $0.56$  (equivalent to power-factors,  $PF$ , of  $4.87 \times 10^{-3}$  and  $2.8 \times 10^{-3}\text{ W K}^{-1}\text{ m}^{-2}$ ) for the  $\text{Bi}_2\text{Te}_3$  and  $\text{Sb}_2\text{Te}_3$  thin-films, respectively. The IC-compatibility and the dependence of the TE performance on technological details, such as photolithography and wet etching used for patterning the thin-films have also been investigated. The converter dimensions for best performance were analysed and a prototype of a planar TE power generator was fabricated.

© 2010 Elsevier B.V. All rights reserved.

### 1. Introduction

Thermocouples are thermoelectric (TE) devices. Conventional thermocouples based on metal wires are cheap, reliable and widely used for measuring high temperatures. This is the case of furnaces, which are widely used in the microelectronic industry. A thermocouple is a simple electric circuit, formed by two dissimilar conductors joined at both ends (i.e. the junctions). Opening the circuit by cutting one of the wires enables the measurement of a voltage, which is proportional to the difference in temperature at the two junctions (the Seebeck effect). Consequently, the thermocouple can be used to generate a voltage proportional to temperature difference without the need of any external electrical bias. A temperature sensor results if one of the junctions is maintained at a well-known temperature. The thermocouple can also be used as an actuator. Applying an electrical current through the thermocouple allows the transportation of heat from one junction (the cold junction) to the other (the warm junction at ambient temperature). As a result, the cold junction is cooled (the Peltier effect) [1]. The Seebeck effect can be used for both temperature (difference) sensing and for realising heat engines to convert heat into electrical energy. The advantages of TE energy conversion is that moving

mechanical parts are avoided, which enables high system reliability, quiet operation and it is usually environmentally friendly. The compact and distributed power is a very attractive feature in a wide range of applications.

However, the TE effect is very inefficient in most materials and the research into special materials is mandatory for practical use. The best performance is obtained in the presence of heavily doped semiconductors, such as the bismuth telluride or the silicon germanium. When using semiconductors, the most desirable situation is when the base materials are both n- and p-doped, since this allows the use of essentially the same material system for fabrication of the two TE legs between the junctions [2]. The selection of materials and the suitable fabrication technologies are further constrained by IC-compatibility requirements in the case of TE power generation in a microsystem, which is the objective of the research presented in this paper. Additional requirements imposed by the microsystem application are: small size, low weight and thermal isolation from the substrate [3].

The functional integration of efficient solid-state TE devices and microelectronic circuits offers many benefits. One is the implementation of local cooling for thermal stabilisation of an on-chip reference element or for reducing leakage current in a critical component such as a photodetector. Another implementation is in TE power generation to enable operation of a low-power circuit without external electric power source, such as a battery. Despite the huge potential of TE self-lowering in autonomous microsystems,

only few approaches to fabricate such microdevices have been reported up to now [4–7].

Due to its compatibility with IC technology, polycrystalline SiGe alloys and polycrystalline Si are commonly used in thermopile applications. Their use in microcoolers has been investigated; however, their performance is very low when compared to that of tellurium compounds, which have been used for many years in conventional large-area Peltier devices [3]. Tellurium compounds (n-type bismuth telluride,  $\text{Bi}_2\text{Te}_3$  and p-type antimony telluride,  $\text{Sb}_2\text{Te}_3$ ) are well-established room temperature TE materials and are widely employed by the industry in conventional TE generators and coolers. Several deposition techniques have been investigated for their suitability for fabricating thin-films materials. The direct evaporation of the bulk materials for the deposition of  $\text{Bi}_2\text{Te}_3$  films was demonstrated by da Silva to be non-suitable. The large differences in vapour pressure of bismuth and tellurium resulted in a compositional gradient along the thin-film thickness [8]. Other techniques explored for the deposition of  $\text{Bi}_2\text{Te}_3$  thin-films are the thermal co-evaporation [9], the electrochemical deposition [10], the co-sputtering [4], the flash evaporation [11] and the metal-organic chemical vapour deposition (MOCVD) [12]. Although all these approaches are in principle suitable, the co-evaporation was used in this work to obtain both the n-type  $\text{Bi}_2\text{Te}_3$  and the p-type  $\text{Sb}_2\text{Te}_3$  thin-films, because it allows to precisely control the stoichiometry of the deposited thin-film with the lowest costs. Only the MOCVD is better than the co-evaporation to obtain thin-films with good uniformity and with the desired stoichiometry. However, in order to do the deposition of thin-films by MOCVD, a reactor chamber is needed. Thus, this process is too expensive and it requires additional security procedures, when compared with the co-evaporation [13].

In this work, both the n-type  $\text{Bi}_2\text{Te}_3$  and the p-type  $\text{Sb}_2\text{Te}_3$  thin-films were obtained by co-evaporation, yielding devices with a TE figure-of-merit,  $ZT$ , of  $0.97$  and  $0.56$ , respectively. The  $\text{Bi}_2\text{Te}_3$  selected samples showed a Seebeck coefficient in the range  $152\text{--}248\text{ }\mu\text{V K}^{-1}$ , resistivity of  $10.6\text{--}16.6\text{ }\mu\Omega\text{ m}$ , a thermal conductivity of about  $1.3\text{ W m}^{-1}\text{ K}^{-1}$  [14], a carrier concentration  $\approx 6 \times 10^{19}\text{ cm}^{-3}$  and a Hall mobility from  $80$  to  $120\text{ cm}^2\text{ V}^{-1}\text{ s}^{-1}$ . The EDX analysis (Energy-Dispersive X-ray spectroscopy) revealed the stoichiometric composition of the selected samples. For the p-type thin-films, the best available results (or selected samples) include Seebeck coefficients in the range  $91\text{--}188\text{ }\mu\text{V K}^{-1}$ , a resistivity of  $7.6\text{--}39.1\text{ }\mu\Omega\text{ m}$ , a thermal conductivity about  $1.7\text{ W m}^{-1}\text{ K}^{-1}$  [14], a carrier concentration  $\approx 4 \times 10^{19}\text{ cm}^{-3}$  and a Hall mobility from  $120$  to  $170\text{ cm}^2\text{ V}^{-1}\text{ s}^{-1}$ . These values are similar to the best values found in the literature for bulk materials [15]. Since bulk materials are used in conventional macro-scale modules, a similar performance of the microconverter is feasible. The performance of a TE device depends on the figure-of-merit,  $ZT$ , of the material, which is given by [3,4,15]:

$$ZT = \frac{\alpha^2}{\rho\lambda} T \quad (1)$$

where  $\alpha$  is the Seebeck coefficient,  $\rho$  the electrical resistivity,  $\lambda$  the thermal conductivity and  $T$  the temperature. Furthermore, the power-factor,  $PF$  ( $\text{W K}^{-1}\text{ m}^{-2}$ ) gives the electric power per unit cross-sectional area of heat flow at a given temperature gradient between the hot and the cold junction. The  $PF$  is given by:

$$PF = \frac{\alpha^2}{\rho} \quad (2)$$

The influence of deposition parameters on the thin-film performance has been studied in detail. For obtaining data that is statistically significant, more than one hundred samples were fabricated. One essential parameter in the fabrication of TE microdevices is the film-to-substrate adhesion. To investigate this issue, three

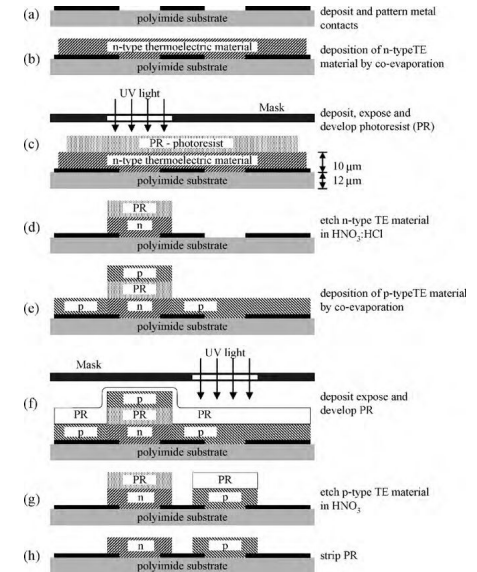


Fig. 1. The fabrication steps of TE devices.

different substrate materials have been used: glass, silicon and polyimide (kapton). However, for actual TE applications, a kapton film was selected as substrate, because of the low thermal conductivity ( $0.12\text{ W m}^{-1}\text{ K}^{-1}$ ). Moreover, the thermal expansion coefficient ( $12 \times 10^{-6}\text{ K}^{-1}$ ) closely matches the thermal expansion coefficient of the telluride thin-films, thus reducing the residual stress and increasing the adhesion. The information obtained on silicon and glass is important for MEMS-based TE devices, where the micromachining is applied for thermal definition of the microstructure. Flexible substrates enable the integration with many novel types of devices, however, also introduce complications, such as the uncommon mechanical properties of the composite film-substrate.

### 2. Fabrication

Two different approaches can be used for the on-chip integration of TE devices: the transversal (off-plane or vertical) and the lateral (in-plane), depending on the direction in which the heat is transported, relative to the surface of the device. In this work, the lateral heat flow is addressed, due to its easier fabrication process and compliance with the planar technology [16]. Fig. 1 shows the process flow used for fabrication of the TE converters.

A thin-layer of metal (aluminium – Al) is deposited by a direct current (DC) sputtering on a polyimide substrate. Then, the patterning of the metal layer is done, and the contacts are obtained (a). Next, the n-type  $\text{Bi}_2\text{Te}_3$  thin-film is deposited by thermal co-evaporation (b). The next step starts with the deposition of a negative photoresist (PR) layer, followed by an expose to UV (ultra-violet) light with a mask made of glass and nickel (to block the UV light) placed between the PR and the UV light source. After the exposition to the UV light, the UV-protected areas will be removed during the PR development (c). The n-type elements are patterned by photolithography (d). The n-type thin-film is etched

\* Corresponding author. Tel.: +351 253 510190; fax: +351 253 510189.  
E-mail address: [jcarmo@dei.uminho.pt](mailto:jcarmo@dei.uminho.pt) (J.P. Carmo).

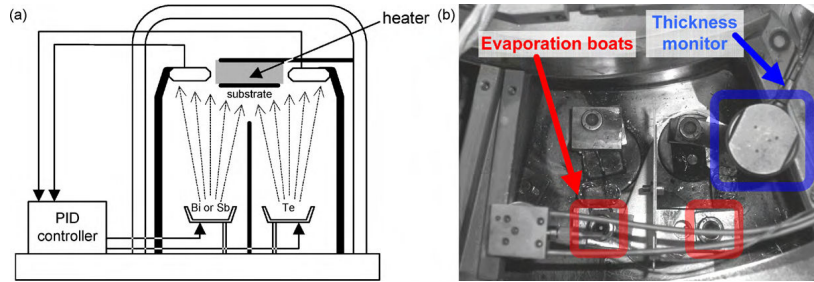


Fig. 2. For the system used in the co-evaporation. (a) A schematic of the complete system, and (b) a photograph showing the inside of the co-evaporation chamber (the two evaporation boats and one of the thickness monitors is visible).

in  $\text{HNO}_3$  and the p-type  $\text{Sb}_2\text{Te}_3$  thin-film is deposited by thermal co-evaporation (e). A new layer of PR is deposited, exposed to a UV light source and developed (f). The TE layer made of  $\text{Sb}_2\text{Te}_3$  is patterned by wet etching in a  $\text{HNO}_3\text{:HCl}$  bath (g) and finally, the PR is removed (h). A protective layer of silicon nitride ( $\text{Si}_3\text{N}_4$ ) can also be deposited by low-temperature hotwire chemical vapour deposition (HW-CVD) and patterned if required by the application.

### 2.1. Deposition of thin-films

TE thin-films were fabricated by thermal co-evaporation (see Fig. 2) in a high-vacuum chamber (with a base pressure of  $\sim 1.33 \times 10^{-4}$  Pa). Two large molybdenum boats (baffled boxes, with a volume of  $4\text{ cm}^3$ ) were used at the same time, one for each of the elementary materials required to produce the desired compound. The power applied to each boat is controlled independently, using two computed proportional-integral derivative (PID) controllers [17] to maintain the deposition rate at user-defined constant values, during the deposition process. Two thickness monitors (quartz crystal oscillators) are carefully placed inside the chamber in such a way that each of them receives material only from the boat it is monitoring. A metal sheet is placed between the two boats to ensure deposition of a material at the respective quartz crystal

sensor only. The substrates are heated to the temperature set point ( $T_{\text{sub}}$ ) in the range  $150\text{--}270^\circ\text{C}$ .

The graphs showing the influence of the evaporation rate,  $R$ , of each material on TE properties of the compounds are presented in Fig. 3. The evaporation flow rate ratio,  $R = F_{\text{Te}}/F_{\text{BiSb}}$ , is defined as the amount (in volume of the deposited film) of tellurium (Te) divided by the amount of bismuth (Bi) – or antimony (Sb) – that arrives the substrate during deposition. The highest power-factor,  $PF$ , was obtained with a Bi (or Sb) evaporation rate of  $2\text{ Å s}^{-1}$  and a Te evaporation rate of  $6\text{--}7\text{ Å s}^{-1}$ , which corresponds to an evaporation flow rate ratio in the range  $3\text{--}3.5$ .

The best values of  $T_{\text{sub}}$  for  $\text{Bi}_2\text{Te}_3$  and for  $\text{Sb}_2\text{Te}_3$  thin-films were about  $270$  and  $220^\circ\text{C}$ , respectively. Finally, it must be noted that all thin-films were deposited on a polyimide (kapton) foil with a thickness of  $25\text{ }\mu\text{m}$ . Fig. 4 shows two SEM cross-section and surface images of both  $\text{Bi}_2\text{Te}_3$  and  $\text{Sb}_2\text{Te}_3$  thin-films, where their polycrystalline structure can be confirmed. Also, the former temperatures and the optimal evaporation flow rate ratios,  $R$ , were those which resulted in thin-films with larger grain size. This is of major concern, because a crystalline structure with an increased grain size is less resistive, whose consequence is a thin-film with an increased TE figures-of-merit,  $ZT$ .

### 2.2. Patterning

TE  $\text{Bi}_2\text{Te}_3$  and  $\text{Sb}_2\text{Te}_3$  thin-films ( $1\text{ }\mu\text{m}$  thick) were deposited on the kapton substrate. The Transene's PKP negative photoresist was applied on the surface, and test structures were patterned by wet etching in the  $\text{HNO}_3\text{:HCl:H}_2\text{O}$  etchant (pure  $\text{HNO}_3$  and 37%  $\text{HCl}$  diluted in water). Fig. 5 shows the influence of the etchant composition on the etch rates. It was observed that an higher per cent of  $\text{HCl}$  ( $\%\text{HCl}/\%\text{HNO}_3 > 0.5$ ) induced cracking of the thin-film, whose consequence is the occurrence of peeling. Fig. 6 shows the influence of etchant dilution (in water) on the etch rate of  $\text{Bi}_2\text{Te}_3$  and  $\text{Sb}_2\text{Te}_3$  thin-films. For the case of  $\text{Bi}_2\text{Te}_3$  thin-films, a dilution above 85% causes the occurrence of peeling. For dilutions below 65%, the etching occurred in a too fast manner and the end of the process was difficult to detect. The best results were obtained with the etchant composition in the range  $10\text{:}0\text{:}25$  to  $10\text{:}5\text{:}40$   $\text{HNO}_3\text{:HCl:H}_2\text{O}$ .

For the case of  $\text{Sb}_2\text{Te}_3$  thin-films, the cracking and peeling of the thin-film occurred when a high percentage of  $\text{HCl}$  was presented in the etchant ( $\%\text{HCl}/\%\text{HNO}_3 > 0.5$ ), as it was observed for the  $\text{Bi}_2\text{Te}_3$  thin-films. The etch rate of the  $\text{Sb}_2\text{Te}_3$  thin-films in diluted  $\text{HNO}_3$  was about 50 times smaller than the etch rate of  $\text{Bi}_2\text{Te}_3$  thin-films in the same etchant. This is important in terms of the selectivity of the process in the presence of both materials. The best results were obtained with the etchant of composition in the range  $10\text{:}1\text{:}20$  to  $10\text{:}6\text{:}40$   $\text{HNO}_3\text{:HCl:H}_2\text{O}$ .

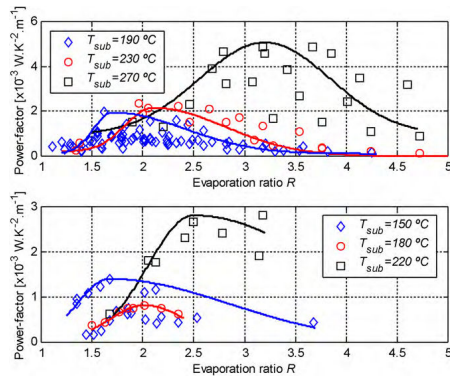


Fig. 3. Power-factor of  $\text{Bi}_2\text{Te}_3$  (top) and  $\text{Sb}_2\text{Te}_3$  (bottom) thin-films as a function of the  $\text{Te/Bi}$  evaporation flow rate ratio,  $R$ , and respective curve fittings (solid lines).

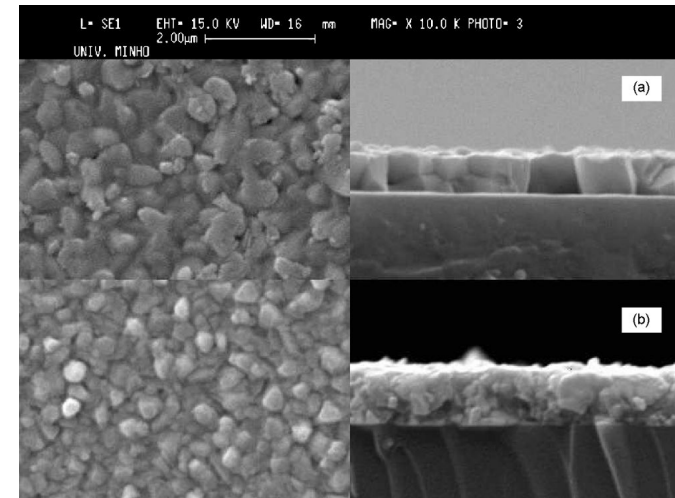


Fig. 4. SEM top view (left) and cross-sectional (right) images of  $\text{Bi}_2\text{Te}_3$  (top)  $\text{Sb}_2\text{Te}_3$  (bottom) thin-films.

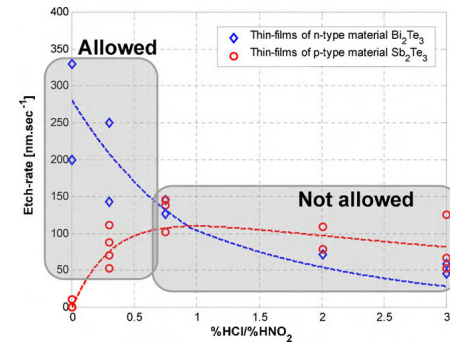


Fig. 5. Etch rate of  $\text{Bi}_2\text{Te}_3$  and  $\text{Sb}_2\text{Te}_3$  thin-films in  $(1-x)\text{HNO}_3\text{:}(x)\text{HCl}$  solution (diluted 70% in water, in volume).

The same solutions for tellurium compounds applied on thin-films made of aluminium resulted in etch rates below  $0.2\text{ nm s}^{-1}$  regardless of the etchant composition. Also, both  $\text{Bi}_2\text{Te}_3$  and  $\text{Sb}_2\text{Te}_3$  were slightly etched ( $<2\text{ nm s}^{-1}$ ) by an aluminium etchant ( $16\text{:}1\text{:}2$  phosphoric acid, nitric acid, acetic acid and water). Table 1 presents all relevant etch rates.

Table 1  
Summary of etch rates.

Etchant	Material			
	$\text{Bi}_2\text{Te}_3$	$\text{Sb}_2\text{Te}_3$	Aluminium	Nickel
Al-Transene type A	$8\text{ Å s}^{-1}$	$5\text{ Å s}^{-1}$	$10\text{--}80\text{ Å s}^{-1}$	$<0.1\text{ Å s}^{-1}$
$3\text{HNO}_3\text{:HCl}$ (dilution 70% $\text{H}_2\text{O}$ )	$2000\text{ Å s}^{-1}$	$800\text{ Å s}^{-1}$	$<2\text{ Å s}^{-1}$	$<0.2\text{ Å s}^{-1}$
$\text{HNO}_3$ (dilution 70% $\text{H}_2\text{O}$ )	$2500\text{ Å s}^{-1}$	$50\text{ Å s}^{-1}$	$<0.1\text{ Å s}^{-1}$	$<0.1\text{ Å s}^{-1}$

Fig. 7 shows a planar TE microconverter, which was fabricated on top of a  $25\text{ }\mu\text{m}$  thickness kapton foil. This microconverter is composed by eight pairs of TE elements and was fabricated with bottom contacts.

### 3. Experimental results

The in-plane thin-film electrical resistance was measured using the conventional four probe van der Pauw method, at the room temperature. The thermal conductivity ( $\text{W m}^{-1}\text{ K}^{-1}$ ) was measured using the method proposed by Völklein [14], and the values of  $1.3$  and  $1.8\text{ W m}^{-1}\text{ K}^{-1}$  were obtained for the  $\text{Bi}_2\text{Te}_3$  and  $\text{Sb}_2\text{Te}_3$  thin-films (which were deposited as conditions to obtain the maximum power-factor), respectively. The measurements of the Seebeck coefficient were made by connecting one side of the thin-film to

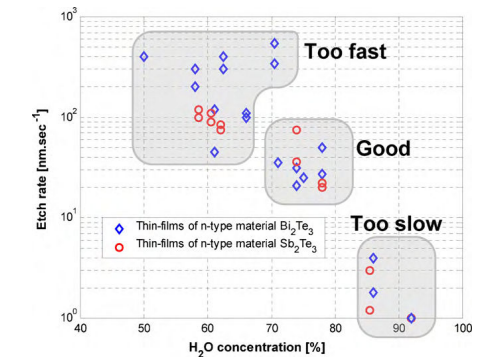


Fig. 6. Etch rate of  $\text{Bi}_2\text{Te}_3$  and  $\text{Sb}_2\text{Te}_3$  thin-films in  $10\text{:}3\text{ HNO}_3\text{:HCl}$  solution, as a function of dilution in water (in volume).

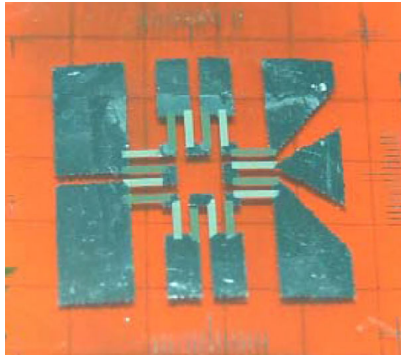


Fig. 7. A photograph of a TE microconverter with eight pairs of TE elements, fabricated with bottom contacts.

a fixed temperature (heated metal block) and the other side to a heat sink at room temperature.

Fig. 8 shows a X-ray diffraction (XRD) spectrum of an optimised  $\text{Bi}_2\text{Te}_3$  thin-film that reveals its polycrystalline structure. The peaks agree with the diffractograms for polycrystalline  $\text{Bi}_2\text{Te}_3$ .

Fig. 9 shows a typical X-ray diffraction spectrum of an optimised thin-film that also reveals its polycrystalline structure. The peaks also agree with the power diffraction spectra for polycrystalline  $\text{Sb}_2\text{Te}_3$ .

Tables 2 and 3 show the results of these measurements in the selected samples of  $\text{Bi}_2\text{Te}_3$  and  $\text{Sb}_2\text{Te}_3$  thin-films, as well as the corresponding figures-of-merit,  $ZT$ . These two following tables also list the  $PF$  for the selected samples of  $\text{Bi}_2\text{Te}_3$  and  $\text{Sb}_2\text{Te}_3$ .

The measurements done in the selected samples showed an absolute value of the Seebeck coefficient in the range of  $91\text{--}248\text{ }\mu\text{V K}^{-1}$ . An in-plane electrical resistivity of  $7.6\text{--}39.1\text{ }\mu\Omega\text{ m}$  was obtained. The measurements for the  $\text{Bi}_2\text{Te}_3$  and  $\text{Sb}_2\text{Te}_3$  thin-films also revealed figures-of-merit,  $ZT$ , at the room temperatures of 0.97 and 0.56, and power-factors,  $PF$ , of  $4.87 \times 10^{-3}$  and  $2.81 \times 10^{-3}\text{ W K}^{-1}\text{ m}^{-2}$ , respectively.

Table 2  
Properties of the selected  $\text{Bi}_2\text{Te}_3$  thin-films.

TF	$T_{\text{sub}}\text{ (}^\circ\text{C)}$	$R = F_{\text{TE}}/F_{\text{RHSb}}$	%Te by EDX	$\alpha\text{ (}\mu\text{V K}^{-1}\text{)}$	$\rho\text{ (}\mu\Omega\text{ m)}$	$PF\text{ (W K}^{-2}\text{ m}^{-1}\text{)}$	$ZT\text{ @ }300\text{ K}$
#1	190	1.70	–	–180	16.6	$1.95 \times 10^{-3}$	0.39
#2	230	2.10	62.8	–156	11.3	$2.16 \times 10^{-3}$	0.43
#3		3.10	62.2	–152	13.4	$1.72 \times 10^{-3}$	0.34
#4	240	3.20	59.1	–180	16.6	$1.95 \times 10^{-3}$	0.40
#5	270	3.20	62.0	–248	12.6	$4.87 \times 10^{-3}$	0.97
#6		3.90	–	–220	10.6	$4.57 \times 10^{-3}$	0.91

Table 3  
Properties of the selected  $\text{Sb}_2\text{Te}_3$  thin-films.

TF	$T_{\text{sub}}\text{ (}^\circ\text{C)}$	$R = F_{\text{TE}}/F_{\text{RHSb}}$	%Te by EDX	$\alpha\text{ (}\mu\text{V K}^{-1}\text{)}$	$\rho\text{ (}\mu\Omega\text{ m)}$	$PF\text{ (W K}^{-2}\text{ m}^{-1}\text{)}$	$ZT\text{ @ }300\text{ K}$
#1	150	1.47	54.5	91	7.6	$1.09 \times 10^{-3}$	0.22
#2		1.67	61.4	140	14.0	$1.40 \times 10^{-3}$	0.28
#3	180	2.02	59.1	158	30.3	$0.82 \times 10^{-3}$	0.16
#4		2.35	62.4	156	39.1	$0.62 \times 10^{-3}$	0.12
#5	220	2.50	67.3	156	9.2	$2.66 \times 10^{-3}$	0.53
#6		3.18	73.5	188	12.6	$2.81 \times 10^{-3}$	0.56

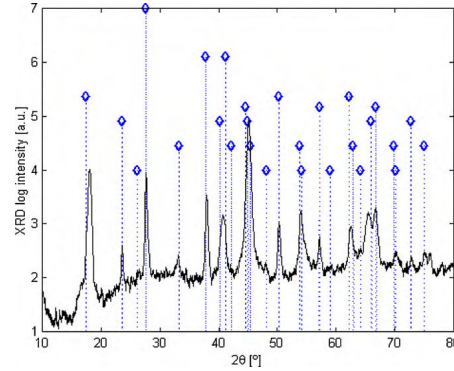


Fig. 8. For a sample of a n-type  $\text{Bi}_2\text{Te}_3$  thin-film XRD analysis. The peaks agree with the power diffraction spectrum for  $\text{Bi}_2\text{Te}_3$  (dotted lines and diamonds).

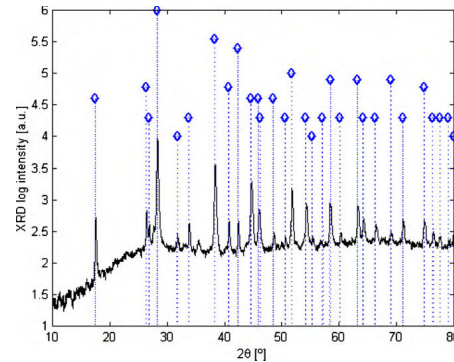


Fig. 9. For a sample of a p-type  $\text{Sb}_2\text{Te}_3$  thin-film XRD analysis. The peaks agree with the powder diffraction spectrum for  $\text{Sb}_2\text{Te}_3$  (dotted lines and diamonds).

#### 4. Conclusions

This paper presented an IC-compatible fabrication technology for thermoelectric (TE) microdevices with high figure-of-merit,  $ZT$ . The deposition of thin-film  $\text{Bi}_2\text{Te}_3$  and  $\text{Sb}_2\text{Te}_3$  materials was done by co-evaporation on kapton substrates. The substrates were submitted to temperatures in the  $190\text{--}270\text{ }^\circ\text{C}$  range in experiments performed to find the best deposition conditions for the  $\text{Bi}_2\text{Te}_3$  thin-films. The substrates also were submitted to temperatures in the range  $150\text{--}220\text{ }^\circ\text{C}$  for thin-films made of  $\text{Sb}_2\text{Te}_3$ . This paper also reported the influence of the deposition parameters on the TE properties of the thin-films. The thin-films were patterned by wet etching in  $\text{HNO}_3\text{:HCl:H}_2\text{O}$  and the influence of the etchant composition in the etch rate and pattern quality was measured. The optimised wet-etching results (i.e. an etch rate of  $100\text{--}200\text{ nm s}^{-1}$  with high selectivity) were obtained with  $10\text{:}3\text{:}30\text{ HNO}_3\text{:HCl:H}_2\text{O}$ . An etch rate below  $0.2\text{ nm s}^{-1}$  was observed in aluminium thin-films, allowing a selectivity higher than 1000. The  $\text{Bi}_2\text{Te}_3$  can also be etched in the  $30\%\text{ HNO}_3$  etchant, with a selectivity higher than 50 as compared to  $\text{Sb}_2\text{Te}_3$  thin-films. The wet etching used is an advantage of the proposed fabrication technology, because of the cost advantage when compared with the reactive ion etching (RIE). Moreover, the etching does not impose limits on substrate temperature during the deposition. The kapton substrate can be bonded to a silicon substrate in a final process step. The IC-compatibility allows the integration with circuits and makes it an enabling technology for the realisation of self-powered wearable microsystems, where the temperature difference between the body temperature and ambient temperature provides sufficient energy for scavenging [18].

#### References

- [1] C. Vining, Semiconductors are cool, *Nature* 413 (October) (2001) 577–578.
- [2] L. Bell, Cooling, heating, generating power, and recovering waste heat with thermoelectric systems, *Science* 321 (September) (2008) 1457–1461.
- [3] D. Wijngaards, S.H. Kong, M. Bartek, R.F. Wolffenbuttel, Design and fabrication of on-chip integrated polySiGe and polySi Peltier devices, *Journal of Sensors and Actuators A: Physical Sensors* 85 (2000) 316–323.
- [4] H. Böttner, J. Nurnus, A. Gavrikov, G. Kühner, M. Jägle, C. Künzel, D. Eberhard, G. Plescher, A. Schubert, K.-H. Schlereth, New thermoelectric components using microsystem technologies, *IEEE Journal of Microelectromechanical Systems* 13 (June (3)) (2004) 414–420.
- [5] L. da Silva, M. Kaviany, Fabrication and measured performance of a first-generation microthermoelectric cooler, *Journal of Membrane Science* 14 (5) (2005) 1110.
- [6] G.J. Snyder, J.R. Lim, C.-K. Huang, J.-P. Fleuria, Thermoelectric microdevice fabricated by a MEMS-like electrochemical process, *Nature Materials* 2 (2003) 528–531.
- [7] H. Böttner, Micropelt miniaturized thermoelectric devices: small size, high cooling power densities, short response time, in: *Proc. 24th International Conference on Thermoelectrics (ICT'05)*, Clemson, SC, USA, June 2005.
- [8] L. da Silva, K. Massoud, Miniaturized thermoelectric cooler, in: *Proc. IMECE'02*, New Orleans, USA, November 2002, pp. 154–161.
- [9] Z. He, D.M. Rowe, S.G.K. Williams, Peltier effect in a co-evaporated  $\text{Sb}_2\text{Te}_3$  ( $\text{P}$ )- $\text{Bi}_2\text{Te}_3$  ( $\text{N}$ ) thin-films thermocouple, *Thin Solid Films*: Elsevier (April 2002) 270–274.
- [10] J. Lim, G.J. Snyder, C.-K. Huang, J.A. Herman, M.A. Ryan, J.-P. Fleuria, Thermoelectric microdevice fabrication process and evaluation at the jet propulsion laboratory, in: *Proc. ICT'2002*, Long Beach, USA, August 2002, pp. 535–539.
- [11] A. Foucaran, Flash evaporated layers of ( $\text{Bi}_2\text{Te}_3\text{--Bi}_2\text{Se}_3$ )( $\text{N}$ ) and ( $\text{Bi}_2\text{Te}_3\text{--Sb}_2\text{Te}_3$ )( $\text{P}$ ), *Materials Science and Engineering B: Elsevier* 52 (1998) 154–161.
- [12] A. Giani, A. Boulouf, F. Pascal-Delannoy, A. Foucaran, E. Charles, A. Boyer, Growth of  $\text{Bi}_2\text{Te}_3$  and  $\text{Sb}_2\text{Te}_3$  thin films by MOCVD, *Materials Science and Engineering B: Elsevier* 64 (1999) 19–24.
- [13] Z.M. Lia, Y. Hao, J.C. Zhang, L.A. Yanga, S.R. Xua, Y.M. Chang, Z.W. Bia, X.W. Zhou, J.Y. Niu, Thermal transport simulation of a susceptor structure with ring groove for the vertical MOCVD reactor, *Journal of Crystal Growth* 311 (December (23–24)) (2009) 4679–4684.
- [14] F. Völklein, Characterisation of the thermal properties of bulk and thin-film materials by using diagnostic microstructures, in: *Proc. Symposium on Microtechnology in Metrology and Metrology in Microsystems*, Delft, The Netherlands, August 2000.

- [15] G. Min, D.M. Rowe, Conversion efficiency of thermoelectric combustion systems, *IEEE Transactions on Energy Conversion* 32 (June (2)) (2007) 528–534.
- [16] K. Tang, K.F. Man, G. Chen, S. Kwon, An optional fuzzy PID controller, *IEEE Transactions on Industrial Electronics* 48 (August (4)) (2001) 757–761.
- [17] D.D.L. Wijngaards, R.F. Wolffenbuttel, Thermo electric characterization of APCVD poly $\text{Si}_0.7\text{Se}_{0.3}$  for IC compatible fabrication of integrated lateral Peltier elements, *IEEE Transactions on Electron Devices* 52 (May (5)) (2005).
- [18] R.F. Yazicioglu, T. Torfs, P. Merken, J. Penders, V. Leonov, R. Puers, B. Gyselsinckx, C.V. Hoff, Ultra-low-power biopotential and their applications in wearable and implantable systems, *Microelectronics Journal* 40 (September (9)) (2009) 1313–1321.

#### Biographies



**João Paulo Carmo** was born in 1970 at Maia, Portugal. He graduated in 1993 and received his MSc degree in 2002, both in Electrical Engineering from the University of Porto, Porto, Portugal. In 2007, he obtained the PhD degree in Industrial Electronics from the University of Minho, Guimarães, Portugal. His PhD thesis was on RF transceivers for integration in microsystems to be used in wireless sensors network applications. Since 2008, he is an Assistant Researcher at the Algoritmi Center, University of Minho. He is involved in the research on micro/nanofabrication technologies for mixed-mode/RF systems, solid-state integrated sensors, microactuators and micro/nanodevices for use in wireless and biomedical applications. Doctor Carmo is also a Member of the IEEE Industrial Electronics Society.



**Luis Miguel Gonçalves** graduated in 1993 and received his MSc degree in 1999, both in Industrial Electronics Engineering from the University of Minho, Guimarães, Portugal. From 1993 to 2002 he researched on embedded systems and electronics, on Idite-Minho, an Institute to interface between University and industry, Braga, Portugal. Since 2002, he has been lecturing at Electronics Department, University of Minho. There, he started a new lab on thermoelectric thin-film deposition, characterization and patterning, in collaboration with Physics department. His PhD thesis was on thermoelectric microsystems for on-chip cooling and energy harvesting. His professional interests are thin-film devices for thermoelectric energy applications, micromachining and microfabrication technology, solid-state integrated microsystems.



**Reinoud F. Wolffenbuttel** received the MSc and PhD degrees from Delft University of Technology, Delft, The Netherlands, in 1984 and 1988, respectively. Between 1986 and 1993, he was an Assistant Professor and, since 1993, he has been an Associate Professor with the Department of Microelectronics, Faculty of Information Technology and Systems, Delft University of Technology, where he is involved in instrumentation and measurement, in general, and on-chip functional integration of microelectronic circuits and silicon sensor, IC process compatible MEMS fabrication, and silicon microsystems, in particular. He was a Visitor at the University of Michigan, Ann Arbor, in 1992, 1999, and 2001, at Tohoku University, Sendai, Japan, in 1995, and at EPFL, Lausanne, Switzerland, in 1997. Professor Wolffenbuttel served as the General Chairman of the Dutch National Sensor Conference in 1996, the Eurosensors in 1999, and the MicroMechanics Europe Workshop in 2003. He was a recipient of the 1997NWO Pioneer Award.



**José Higinio Correia** graduated in Physical Engineering from University of Coimbra, Portugal in 1990. He obtained in 1999 a PhD degree at the Laboratory for Electronic Instrumentation, Delft University of Technology, The Netherlands, working in the field of microsystems for optical spectral analysis. Presently, he is a Full Professor in Department of Industrial Electronics, University of Minho, Portugal. He was the General Chairman of Eurosensors 2003 and MME 2007, Guimarães, Portugal. His professional interests are in micromachining and microfabrication technology for mixed-mode systems, solid-state integrated sensors, microactuators and microsystems. Professor Correia is also a Member of the IEEE Industrial Electronics Society.